SECED 2023 Conference
Earthquake Engineering & Dynamics for a Sustainable Future
14-15 September 2023, Cambridge, UK

FAULT-ORIENTED SPATIALLY DISTRIBUTED SEISMICITY MODEL AND COSEISMIC LANDSLIDE HAZARD ASSESSMENT FRAMEWORK FOR UGANDA

Morris OLENG[1], Zuhal OZDEMIR[2] & Kypros PILAKOUTAS[3]

Abstract: *Uganda's location between the western and eastern branches of the East African Rift System exposes several parts of the Sub-Saharan African country, which already suffers from landslides, to earthquakes of varying degrees. Over the past decades, many destructive seismic events e.g., the 1929 Masaka, 1966 Toro, 1994 Kisomoro and 2016 Bukoba earthquakes have caused enormous human and economic losses. Moreover, the catastrophic impacts of these events have been exacerbated by the triggered landslides around earthquake epicentres. The proliferation of a substandard building stock caused by lack of building control and obsolete seismic design guidelines coupled with rapid population growth and urbanisation exposes Uganda to a massively increasing risk from such disasters. Hence, there is an urgent need to quantify this risk so that mitigation measures can be applied. In retrospect, as the first step towards the development of a seismic risk and resilience assessment framework for Uganda, this paper holistically presents a stochastic probabilistic seismic multi-hazard model developed based on fault-oriented and spatially distributed seismicity data for Uganda. Suitable attenuation relationships are implemented using a logic tree approach to predict ground motion in both stable continental and active shallow crust geological formations. Herein, the multi-hazard assessment tool incorporates coseismic landslides into the framework for Uganda. Mean seismic hazard maps in terms of PGA are computed for 475 and 2475-year return periods, in addition to a probabilistic assessment of coseismic landslides based on various conditioning factors. The findings, which are generally consistent with previous regional studies, indicate that western Uganda is prone to higher seismicity and coseismic landslides compared with the other parts of the country. Correspondingly, the framework presented herein can be used to kick-start the update and continuous improvement of Uganda Seismic Design Code, as well as help develop a National Seismic Mitigation Strategy.*

Introduction

In many developing countries, the severity of natural disasters like earthquakes, landslides and floods is increasing tremendously. The devastating damage to the built and natural environment results in huge economic losses, thereby affecting human welfare (Corominas et al., 2014; Petley, 2012). In Uganda, many socio-economic sectors e.g., health, education, infrastructure and institutional governance have suffered consequentially. Over the past decades, many destructive disasters occurred in several parts of Uganda, resulting in deaths, injuries, physiological distress and damage to property. Although Uganda faces numerous disasters, earthquakes and landslides are largely responsible for the majority of deaths related to socio-natural disasters across the country (Doocy et al., 2013; Kato & Mutonyi, 2011).

Destructive earthquakes in East Africa are largely driven by the world's largest seismically active continental rift i.e., the East African Rift System (EARS) (Asefa & Ayele, 2021; Midzi et al., 1999). The most recent 2016 Bukoba earthquake of M_w 5.9 left many Ugandans homeless and resulted in high economic losses. This event caused 11 deaths, over 440 injures and economic losses worth US$ 458 million estimated in Kagera region (Balikuddembe & Sinclair, 2018). Another case in point is the emergence of hot springs in Buranga when the 1994 Kisomoro earthquake with M_s 6.2 hit Bundibugyo, Kabarole and Kasese districts (Cheriberi & Yee, 2022; Midzi & Manzunzu, 2014). This earthquake killed 8 people and caused several injuries with economic losses estimated at US$ 60 million (Kahuma et al., 2006). In 1945, an earthquake of M_s 6.0 resulted in 5 deaths, several injuries and building collapses in Masaka (Bisset, 1945; Loupekine, 1966). The

[1] Doctoral Researcher, The University of Sheffield, Sheffield, UK, MOleng1@sheffield.ac.uk
[2] Lecturer, The University of Sheffield, Sheffield, UK
[3] Professor, The University of Sheffield, Sheffield, UK

worst event this century (1966 Toro earthquake of M_s 6.6) hit western Uganda and caused 160 deaths, 1,300 injuries, and damaged more than 7,000 houses (Sykes, 1967). The 1929 Masaka earthquake of M_b 5.9, which was accompanied by numerous foreshocks and aftershocks, was broadly felt across Uganda. Moreover, earthquake-triggered landslides occurred extensively in the epicentral region and changes in hot springs were observed (Maasha, 1975).

Over the past few decades, there has been wider reporting of landslides across Uganda due to the increasing frequency of events in the region (DesInventar, 2020). However, not all landslide events reported are triggered by earthquakes. The majority of landslides are induced by rainfall and other land use factors which have consequentially led to destruction of the ecosystem and infrastructure like schools, bridges and homesteads (Masaba et al., 2017). A case in point is the March 2010 landslide which occurred in Bududa district in eastern Uganda. At least 388 people died in this unprecedented disaster, with over 8500 people affected (Broeckx et al., 2019). In the western part of the country, several rainfall-triggered and coseismic landslides have caused over 56 deaths, leaving over 14,000 people destitute, in addition to the destruction of crops, livestock, buildings and damage to road infrastructure (Jacobs et al., 2016). While predisposing factors e.g., geology and topography often account for initiation of slope instability, many past studies indicate that these landslides have largely been triggered by rainfall and earthquakes (Knapen et al., 2006).

Even though past earthquakes and landslides have resulted in relatively small losses, damages are likely to escalate due to rapid population growth and urbanisation. According to the most recent census, Uganda's population is estimated at over 41.6 million (UBoS, 2020). Moreover, increased losses may arise due to the largely substandard building stock and recent adoption of more rigid structural systems which are more vulnerable when poorly engineered and executed (Vicente et al., 2011). Notwithstanding the fact that Uganda already suffers from floods, the proliferation of substandard constructions coupled with rapid population growth and urbanisation exposes much of the country's territory to an increasing risk from earthquakes and landslides. Hence, there is an urgent need to quantify this risk so that mitigation measures can be taken. As the first step towards the development of a seismic risk and resilience assessment framework for Uganda, this paper presents a Monte Carlo (MC) based probabilistic seismic hazard model which incorporates coseismic landslides into the framework for the country. Seismic source and ground motion characterisation of site response is implemented using fault-oriented spatially smoothed seismicity technique.

Geology and tectonics of Uganda

Uganda's location between the two active arms of the EARS offers an ideal basis for observing processes (e.g., geology, tectonics and seismicity) associated with the rift system. With extensive variations, the country has recorded a long geological timescale of more than three billion years (Schlüter, 2008). The geology of Uganda (Figure 1) largely comprises Neo and Mesoarchean lithospheric fragments welded by Palaeo, Meso and Neoproterozoic fold belts.

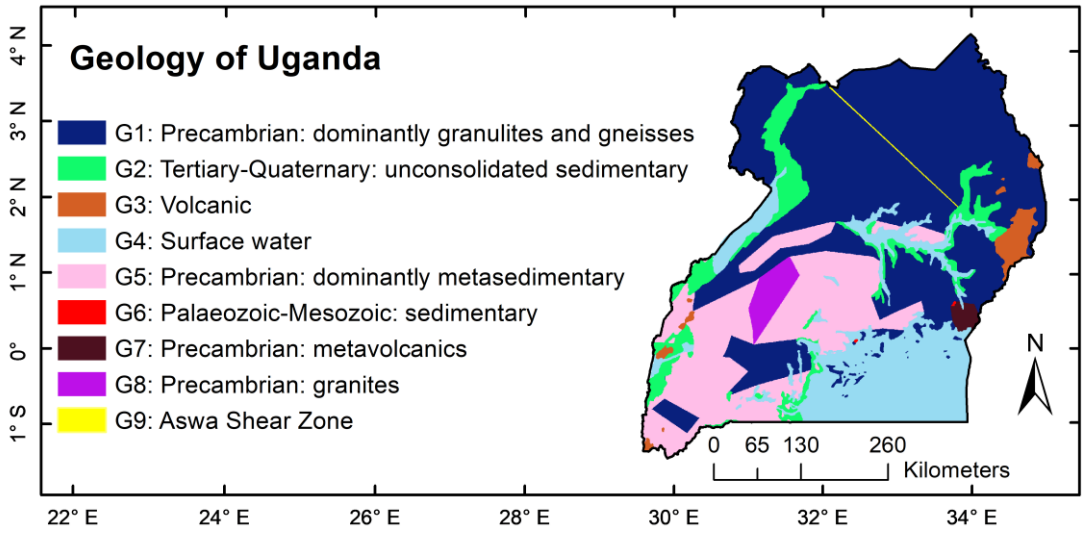

Figure 1. Simplified geological map of Uganda

The major geo-tectonic feature responsible for Uganda's seismicity is the EARS. Its geology basically comprises of Precambrian metamorphic rocks, sedimentary rocks of Miocene age, and a series of Neogene and quaternary lacustrine and fluvial deposits. The western branch of EARS, whose basins are occupied by large lake systems, composes of a series of linked half-graben basins that are typically 80 to 160 km long and 30 to 60 km wide. Another geo-tectonic feature, which stretches from the boughs of Rwenzori Mountains in western Uganda, is the Rwenzori Fold Belt (RFB). Geological evidence indicates that faulting along the RFB continues across Lake Victoria to Speke Gulf and Kavirondo rift; and terminates across the Tanzanian boarder. The geology of RFB largely comprises Paleoproterozoic low to high grade metamorphic rocks of the Buganda-Toro system and selected sediments of undifferentiated Granites. The other parts constituting the Uganda shield have recorded little seismicity in the past. The predominant feature in this region is the largely stable and inactive *Aswa* shear zone which stretches from Nimule to the foothills of Mount Elgon.

Uganda earthquake catalogue

Earthquake catalogue compilation and duplicate removal

In PSHA, earthquake catalogues are required to quantify seismicity, determine source zonation, and compute recurrence parameters associated with earthquakes in the region of interest. The first earthquake catalogue was obtained locally from the Directorate of Geological Survey and Mines in Uganda. However, because of large solution uncertainties, catalogues from other credible global agencies like ISC-GEM (Di Giacomo et al., 2018; Storchak et al., 2013; Storchak et al., 2015), USGS database, ISC reviewed bulletin (ISC, 2022) and GEM global historical earthquake archive (Albini et al., 2013) were obtained. Additional catalogues were derived from the reappraisal of major African earthquakes between 1900 and 1930 (Ambraseys & Adams, 1991), and the compilations by Maasha (1975).

Since several sources were used to compile the Uganda earthquake catalogue, suitable time and space windows of 120 seconds and 55.5 km (approx. 0.5^{o}) suggested by Poggi et al. (2017) were used to identify and remove duplicate events before catalogue refinement. Subsequently, the updated Uganda catalogue was produced using the catalogue toolkit (Weatherill et al., 2016).

Catalogue refinement

1. Homogenisation: For consistency when specifying rupture rates and ground shaking intensities, the moment magnitude (M_w) scale is often preferred partly due to its relation to seismic moment. In this work, earthquake magnitudes were harmonised using magnitude conversion equations proposed by Weatherill et al. (2016), Edwards et al. (2010) and Engdahl and Villaseñor (2002). Subsequently, Figure 2 shows the temporal distribution of both *Poissonian* and dependent events in the homogenised catalogue for Uganda.
2. Declustering: Although seismic hazard analysis essentially assumes to describe seismicity using a *Poisson* model in which the instantaneous occurrence of events is independent, earthquake sequences often feature many foreshocks and aftershocks which are related to the mainshocks. In addition to the modified Knopoff (2000) algorithm extended by Bustos (2009), the original Gardner and Knopoff (1974); together with its subsequent modifications by Gruenthal (van Stiphout et al., 2012) and Uhrhammer (1986) were run to remove clustered/correlated events. The number of mainshocks and dependent events in the refined catalogue according to each algorithm is listed in Table 1. As a conservative approach for estimating the associated seismicity parameters, subsequent analysis was based on the declustered catalogue using the modified Knopoff (2000) algorithm.

Algorithm	Mainshocks	Events removed	Percentage of events removed (%)	Clusters
Gardner and Knopoff (1974)	365	379	50.54	101
Gruenthal (van Stiphout et al., 2012)	309	435	58.13	98
Uhrhammer (1986)	511	233	30.76	70
Musson (1999)	485	259	34.28	76
Modified Knopoff (2000)	543	201	27.02	99

Table 1. Summary of non-Poissonian events removed using various declustering algorithms

3. Completeness analysis: Earthquake catalogue completeness procedures analysed for different time periods and completeness thresholds may vary for each magnitude range. In this work, the original Stepp (1972) procedure gave erroneous results possibly due to the

sparse and largely irregular data coverage. Subsequently, the MATLAB code of Wiemer (2001) was executed to statistically evaluate completeness magnitudes and their period thresholds using the maximum curvature method (Wiemer & Wyss, 2000) and *b-value* stability approach (Cao & Gao, 2002) in combination with a bootstrapping mechanism. Figure 2 also shows a magnitude-time density plot with normalised rates computed for a 0.1 magnitude bin and fixed time window of 5 years. The *red* lines denote the completeness magnitudes and their periods. The incomplete period was rejected in subsequent analyses.

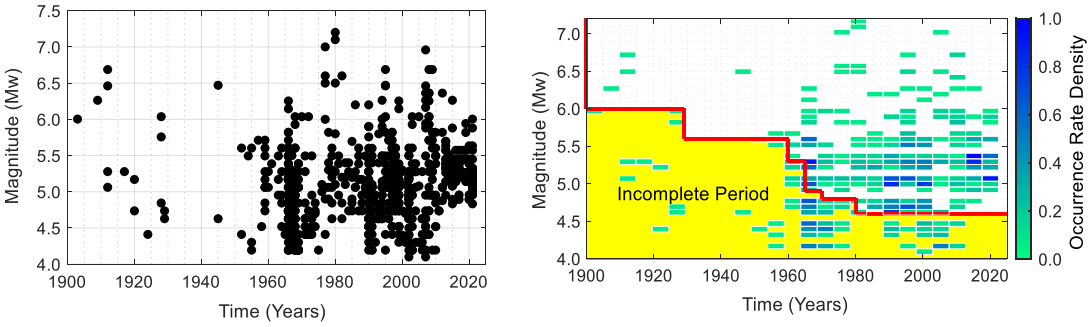

Figure 2. Distribution of seismicity over time for the events in the homogenised non-declustered catalogue; and magnitude-time-density plot of the Uganda catalogue.

Landslide inventory data

Digital Elevation Model (DEM)

Although elevation data compiled for the period between 1962 and 1970 was initially acquired from Uganda National Forest Authority, updated Shuttle Radar Topography Mission (SRTM) data at 30-metre resolution was obtained from a more recent database (RCMRD, 2022). This elevation dataset shown in Figure 3 was used to model predisposing (topographical or geomorphological) factors like slope angles, slope aspect and slope position etc.

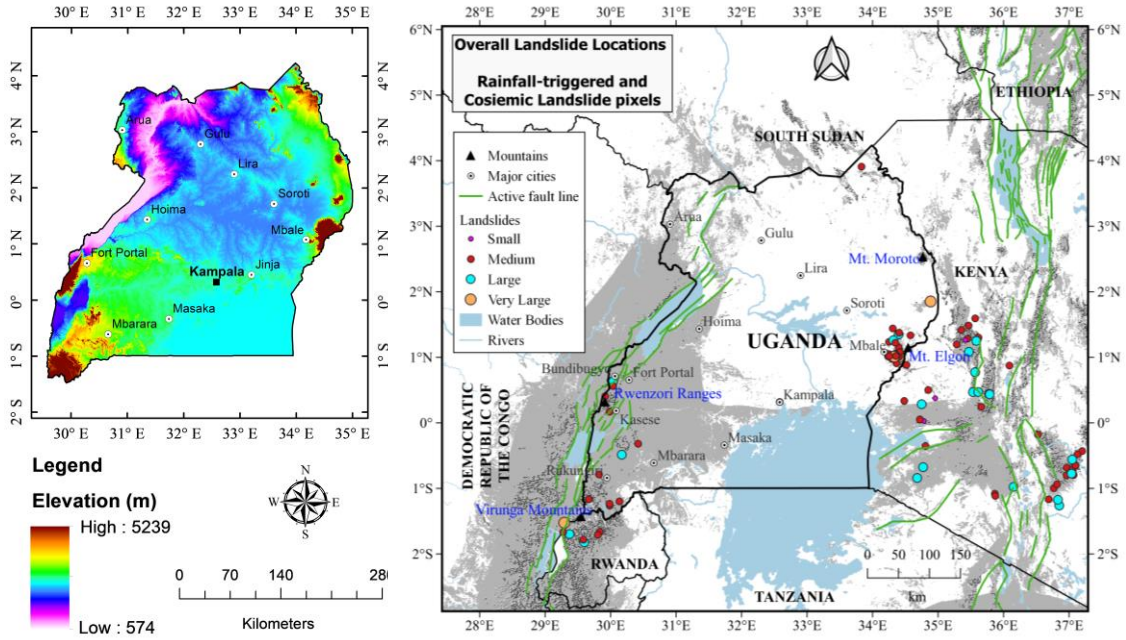

Figure 3. Digital Elevation Model (DEM) at 30m SRTM resolution; and overall landslide locations superimposed on coseismic and rainfall-triggered landslide pixels for Uganda

Landslide location and pixel distribution

In order to map the overall landslide hazard locations for Uganda, rainfall-triggered ground failure inventories and data on earthquake-induced landslides were obtained from the NASA satellite data and USGS repository respectively (NASA, 2022; USGS, 2022). Landslide hazard pixel data was obtained from the online database of World Bank and Global Facility for Disaster Reduction and Recovery (WorldBank & GFDRR, 2022). As seen in Figure 3, the mountainous parts of the

country, particularly the Elgon and Rwenzori mountains, have experienced more landslides with a greater concentration of landslide clusters because of the high annual precipitation (Bamutaze, 2011), and steep slopes of relatively low shear resistance (Nakileza & Nedala, 2020). The fault system indicated in Figure 3 was obtained from the database by Styron and Pagani (2020).

Methodology

Monte Carlo (MC) based PSHA

Herein, the stochastic event-based PSHA calculator for distributed seismicity embedded in the *OpenQuake*-engine (Pagani et al., 2014) was employed to determine sample realisations from each intensity measure for a given scenario. Although its computation cost is high, MC simulation approach allows for model flexibility and is convenient when applying physics-based attenuation models (Graves et al., 2011). Comprehensive descriptions of MC-based PSHA may be found in literature by Musson (1999), Crowley and Bommer (2006) and Baker et al. (2021) etc.

Seismic source characterisation

A typical strategy which involves preparing the earthquake catalogue, dividing the region into geo-tectonic domains, choosing and defining source geometries and typologies, and assigning activity rates to each zone (Vilanova et al., 2014) was used in this work. Consequently, as shown in Figure 4, the zonation adopted 13 area source zones (ASZs). Because certain zones recorded very few events, ASZs of similar geo-tectonics were grouped to statistically give reliable estimates of recurrence. Calibrated seismicity parameters, defined within the Gutenberg-Richter recurrence law, were estimated using the maximum likelihood algorithm of Weichert (1980). Realistic estimates of maximum magnitudes (M_{max}) were obtained by adding conservative increment of 0.5 magnitude units to the maximum observed magnitude for each area source zone.

Logic tree implementation

In this work, the functionalities embedded in GEM Ground Motion Toolkit (Weatherill et al., 2014) were utilised to select four attenuation models. For active shallow crust: AA- Akkar et al. (2014) and CY- Chiou and Youngs (2014) models were applied; while PA- Pezeshk et al. (2011) and AB-Atkinson and Boore (2006) models were adopted for stable continental crust formations. Epistemic uncertainties associated with the model were minimised by implementing a logic-tree with weights assigned according to the likelihood of each clustered tectonic type as shown in Table 2.

Landslide frequency ratio

A statistical bivariate method was used to calculate the spatial relationship between landslide conditioning factors and the location of landslides in the study region. Landslide frequency ratio (FR) described in Eq. 1 is defined as the relative landslide frequency within a given landslide conditioning factor in comparison with the relative landslide frequency in the overall study area.

In Eq. 1, $N^p{}_i$ is the number of landslide pixels in landslide conditioning factor class, N^l is the total number of pixels in the landslide conditioning factor, N^{lp} is the total number of landslide pixels in the study area, and N is the total number of pixels in the study area (Yilmaz, 2009).

$$FR = \frac{N^p{}_i / N^l}{N^{lp} / N} \tag{1}$$

Semi data-driven fuzzy memberships

Owing to Uganda's substantial lack of historical landslide inventory, this study employed a fuzzy logic based approach for coseismic landslide hazard assessment executed in a *GIS* environment (Kritikos et al., 2015). Several fuzzy membership functions in the fuzzy membership tool embedded in *ArcGIS 10* (Raines et al., 2010) were used to produce fuzzy maps. The *fuzzy GAMMA* operator (Eq. 2) was used to generate membership functions for the related coseismic and rainfall-triggered landslide conditioning factors.

$$\mu(x) = \left[1 - \prod_{i=1}^{n}(1-\mu_i)\right]^{\gamma} - \left[\prod_{i=1}^{n}\mu_i\right]^{1-\gamma} \tag{2}$$

where $\mu(x)$ is the combined membership function, μ_i is the fuzzy membership function for the i^{th} fuzzy overlay map, and the parameter γ is chosen in the range of 0 and 1.

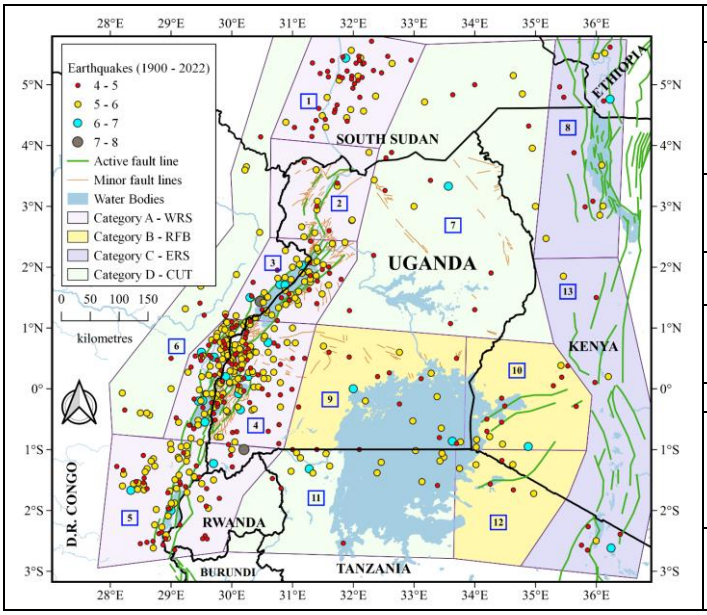

Group	ASZs	M_{max}	a-value	b-value
WRS	1	6.7	3.080	0.96
	2	6.4	7.937	
	3	7.6	3.056	
	4	7.2	3.645	
	5	7.7	3.216	
RFB	9	7.0	1.721	0.86
	10	7.0	2.276	
	12	6.1	4.576	
ERS	8	6.7	2.935	0.79
	13	7.0	2.107	
CUT	6	6.2	1.683	0.67
	7	7.0	2.466	
	11	6.6	1.978	

WRS – Western Rift System;
RFB – Rwenzori Fold Belt;
ERS – Eastern Rift System;
CUT – The Uganda Shield.

For all ASZs, the minimum magnitude threshold of Mw = 4.0 was used.

Figure 4. Earthquake epicentres, faults, area source zonation model; and seismicity parameters used in the performance of MC based PSHA for Uganda.

Source Group	ASZs	Active Shallow Crust		Stable Continental Crust	
		AA	CY	PA	AB
WRS	1, 2, 3, 4, 5	0.250	0.250	0.250	0.250
RFB	9, 10, 12	0.375	0.375	0.125	0.125
ERS	8, 13	0.000	0.000	0.500	0.500
CUT	6, 7, 11	0.500	0.500	0.000	0.000

Table 2. Weighting scheme used for the attenuation model logic tree implementation

Results and discussion

MC-based PSHA

Considering 5% damped response spectral acceleration, target ground motion intensities are derived for a 50-year investigation time to estimate 10% and 2% probabilities of exceedance (POE), corresponding to 475 and 2475-year return periods respectively. With a mesh spacing of 2.5km, the investigated area comprises of a total of 16,637 sites including the buffer zone. Site conditions were modelled using the upper 30-metre averaged shear-wave velocity reference data derived by Allen and Wald (2007). Accordingly, seismic hazard maps in terms of peak ground acceleration (PGA) for the given return periods were prepared as shown in Figure 5.

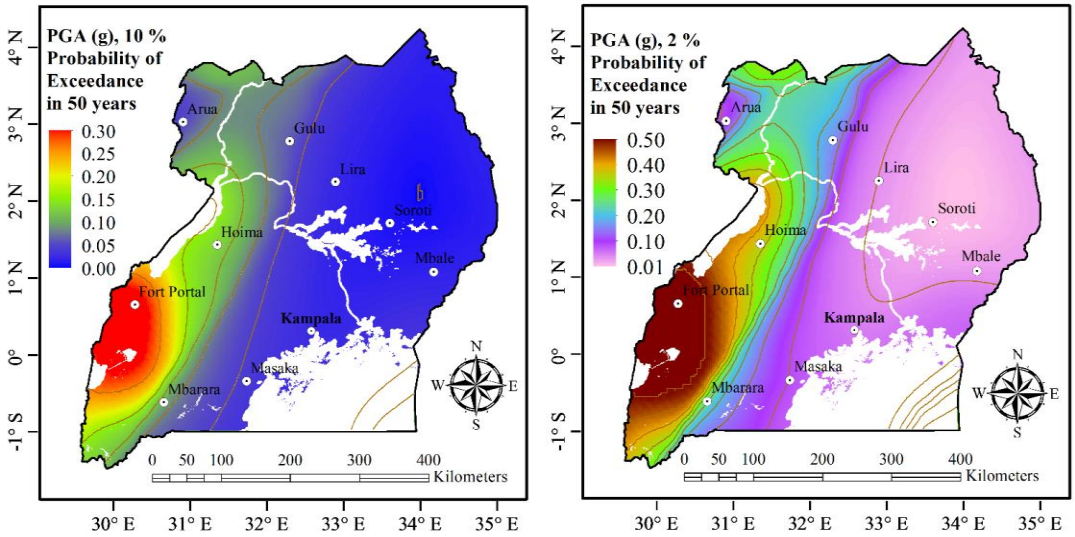

Figure 5. Uganda seismic hazard maps (contours imposed at 0.05 g intervals) investigated over 50 years period, in terms of PGA and computed for 475 and 2475-year return periods.

The result shows that Albertine, Rwenzori and Upper Kivu regions (ASZs 3 and 4) can expect a maximum PGA of 0.3 g and 0.5 g for 10 % and 2 % POE in 50 years respectively; whilst the rest of the country has relatively lower accelerations. These values closely match the predictions in previous regional studies e.g., GSHAP project (Midzi et al., 1999) and the GEM and *AfricanArray* project (Poggi et al., 2017). Given the recent spike in population, urbanisation and increased economic activity in these regions, the overall risk has significantly increased.

Landslide frequency ratio

Topography, hydrology and geo-tectonic factors were considered in the prediction of landslide hazard in Uganda. An assessment of the distribution of landslide frequency for predisposing factors of slope angle, slope aspect, slope position, distance from streams, proximity to active faults, and geology is shown in Figure 6. It is observed that steeper slopes are more susceptible to failure due to greater vertical component of gravity which results in increased shear stresses in the soil. Based on the slope orientation/direction, landslide occurrence is equally distributed across the country. Regarding slope position, the majority of the country's territory consists of lower slopes, with the western and eastern boundaries predominantly comprising of flat and middle slopes. Notably, the mountainous regions where many landslides have occurred are largely dominated by upper slopes and ridges. Also, the inclusion of hydrology takes into account the undercutting stream flow, stream channel and gulley erosion, and terrain modification.

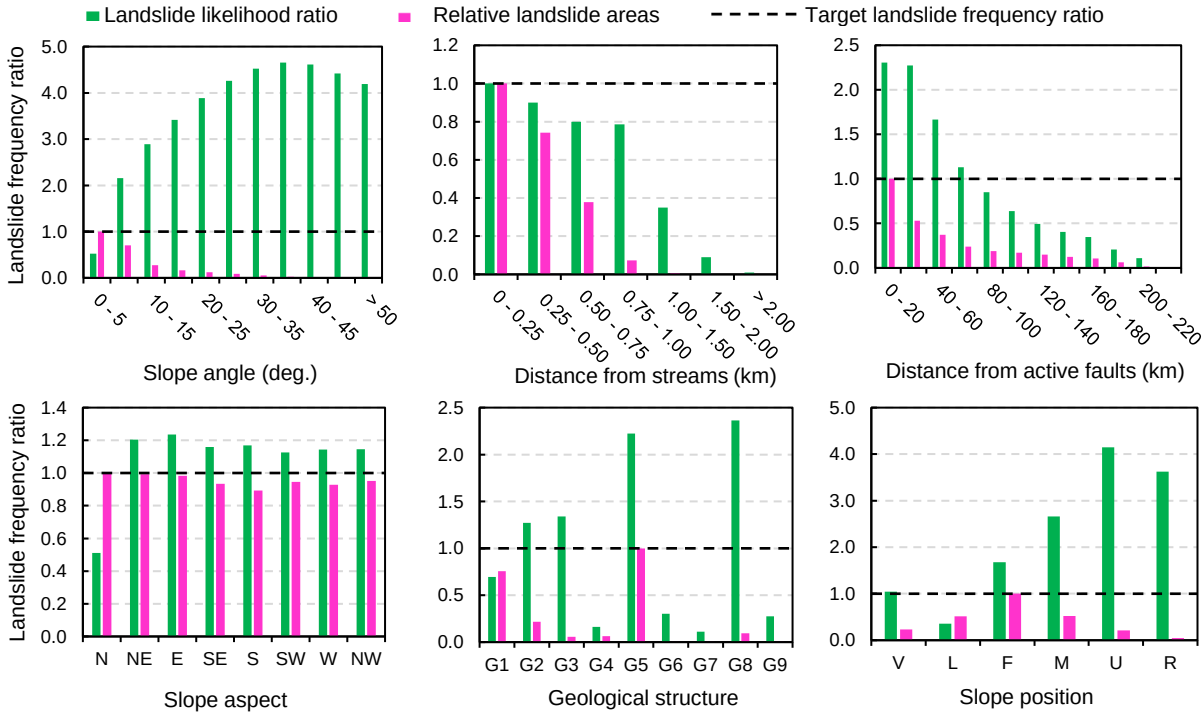

Legend. *Slope Aspect* – N: North, NE: Northeast, E: East, SE: Southeast, S: South, SW: Southwest, W: West, and NW: Northwest; *Geological formation* – G1: Precambrian (dominantly granulites and gneisses), G2: Tertiary-Quaternary (unconsolidated sedimentary), G3: Volcanic, G4: Surface water, G5: Precambrian (dominantly metasedimentary), G6: Palaeozoic-Mesozoic (sedimentary), G7: Precambrian (metavolcanics), G8: Precambrian (granites), and G9: Aswa Shear Zone; *Slope position* – V: Valley, L: Lower slope, F: Flat slope, M: Middle slope, U: Upper slope, and R: Ridge

Figure 6. Landslide frequency ratios and their relative areas for predisposing conditioning factors of slope angle, distance from streams, proximity to active faults, slope aspect, geology, and slope position. The black dashed lines indicate a target FR of 1.0.

As it is seen in Figure 6, regions closer to streams have experienced more landslides. Similarly, regions closer to active faults are more vulnerable to coseismic landslides. This is due to the likelihood of seismic energy release which causes significant reduction in soil/rock strength along fault traces. Moreover, a correlation of landslides and the geology of Uganda shows that regions of Precambrian granites and predominantly metasedimentary structures exhibit higher landslide frequency ratios.

Intermediate coseismic landslide susceptibility mapping

Using the *fuzzy Gamma* overlay tool embedded in *ArcGIS*, the aggregated fuzzy factor maps for a combination of PGA and selected conditioning factors were produced (Figure 7). The hazard assessment maps quantitatively show the probability of coseismic landslides for each pixel across Uganda. Each conditioning factor was correlated with a PGA computed for 10% POE in 50 years (475-year return period). The results generally indicate that western Uganda, which is more seismically active, has the highest chance of experiencing earthquake-triggered landslides.

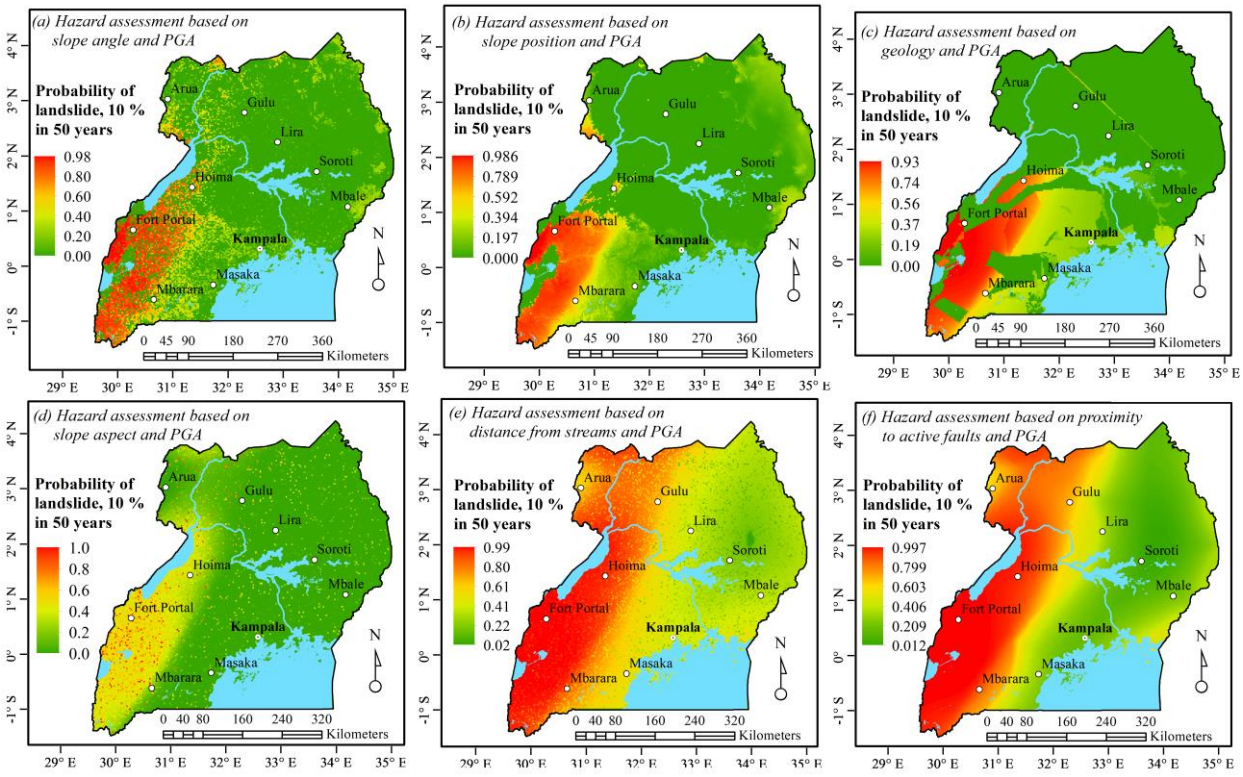

Figure 7. Probability of coseismic landslides for return period of 475 years, based on the various conditioning factors and PGA (g) across Uganda.

Conclusion

This paper presents a novel MC-based PSHA framework for Uganda and the model developed herein incorporates rainfall-triggered and coseismic landslides occurring across the country's territory. An updated earthquake catalogue for Uganda was compiled from credible sources prior to the refinement process. Seismic source zones were delineated based on past seismicity, geology and seismo-tectonic setting of Uganda. Then, a maximum likelihood method was used to estimate recurrence parameters. In the prediction of ground motion while catering for epistemic uncertainties in clustered tectonic regions, a logic tree was implemented to appropriately assign weights to selected attenuation models. An updated elevation model and landslide scars were used to model triggering and predisposing landslide conditioning factors. Although the outputs of this work confirm that western Uganda is exposed to highest level of earthquake and subsequent coseismic landslide hazards, several parts of the country are prone to similar disasters of varying degrees. The holistic seismic hazard assessment framework presented herein can reliably be used to kick-start the update and continuous improvement of a more robust seismic design code for Uganda. In retrospect, the developed hazard model can be incorporated into a multi-hazard earthquake risk assessment framework, aimed at providing policymakers, practitioners, insurance companies and government stakeholders with practical risk appraisal techniques geared towards reducing future landslide and earthquake-related losses in the country.

Acknowledgements

The authors are wholly responsible for the contents herein and special thanks goes to the Directorate of Geological Surveys and Mines (DGSM) under the Ministry of Energy and Mineral Development (MEMD) who provided the initial earthquake data for Uganda.

References

Akkar, S., Sandıkkaya, M. A., & Bommer, J. J. (2014). Empirical ground-motion models for point-and extended-source crustal earthquake scenarios in Europe and the Middle East. *Bulletin of earthquake engineering*, *12*(1), 359-387.

Albini, P., Musson, R., Gomez Capera, A., Locati, M., Rovida, A., Stucchi, M., & Viganò, D. (2013). Global historical earthquake archive and catalogue (1000-1903). *Pavia, Italy*. https://www.emidius.eu/GEH/map.php

Allen, T. I., & Wald, D. J. (2007). Topographic slope as a proxy for global seismic site conditions ($V_{S,30}$) and amplification around the globe. *U.S. Geological Survey Open-File Report 2007-1357, 69 p.*

Ambraseys, N., & Adams, R. (1991). Reappraisal of major African earthquakes, south of 20° N, 1900–1930. *Natural Hazards*, *4*(4), 389-419.

Asefa, J., & Ayele, A. (2021). Seismicity of the East African Rift System for the period 2013 to 2016. *Journal of African Earth Sciences*, *183*, 104315.

Atkinson, G. M., & Boore, D. M. (2006). Earthquake ground-motion prediction equations for eastern North America. *Bulletin of the seismological society of America*, *96*(6), 2181-2205.

Baker, J., Bradley, B., & Stafford, P. (2021). *Seismic hazard and risk analysis*. Cambridge University Press.

Balikuddembe, J. K., & Sinclair, P. (2018). Uganda at glance of 5.7 magnitude earthquake: lessons for earthquake risk reduction. *PLoS currents*, *10*.

Bamutaze, Y. (2011). Patterns of water erosion and sediment loading on Mt. Elgon, Eastern Uganda. *Geography. Makerere University, Kampala*.

Bisset, C. (1945). Notes on earth tremor on and about 18 March 1945. *Bull. Uganda Soc*, *4*, 25-28.

Broeckx, J., Maertens, M., Isabirye, M., Vanmaercke, M., Namazzi, B., Deckers, J., Tamale, J., Jacobs, L., Thiery, W., & Kervyn, M. (2019). Landslide susceptibility and mobilization rates in the Mount Elgon region, Uganda. *Landslides*, *16*(3), 571-584.

Bustos, A., Guillermo. (2009). *An exploratory study of parameter sensitivity, representation of results and extensions of PSHA: case study-United Arab Emirates* Imperial College London].

Cao, A., & Gao, S. S. (2002). Temporal variation of seismic b‐values beneath northeastern Japan island arc. *Geophysical research letters*, *29*(9), 48-41-48-43.

Cheriberi, D., & Yee, E. (2022). Preliminary Seismic Hazard Analyses for the Ugandan Region. *Applied Sciences*, *12*(2), 598.

Chiou, B. S.-J., & Youngs, R. R. (2014). Update of the Chiou and Youngs NGA model for the average horizontal component of peak ground motion and response spectra. *Earthquake spectra*, *30*(3), 1117-1153.

Corominas, J., van Westen, C., Frattini, P., Cascini, L., Malet, J.-P., Fotopoulou, S., Catani, F., Van Den Eeckhaut, M., Mavrouli, O., & Agliardi, F. (2014). Recommendations for the quantitative analysis of landslide risk. *Bulletin of engineering geology and the environment*, *73*(2), 209-263.

Crowley, H., & Bommer, J. J. (2006). Modelling seismic hazard in earthquake loss models with spatially distributed exposure. *Bulletin of earthquake engineering*, *4*(3), 249-273.

DesInventar. (2020). *The national disaster loss database* https://www.desinventar.net/DesInventar/profiletab.jsp (accessed 24.08.2022)

Di Giacomo, D., Engdahl, E. R., & Storchak, D. A. (2018). The ISC-GEM earthquake catalogue (1904–2014): status after the extension project. *Earth System Science Data*, *10*(4), 1877-1899.

Doocy, S., Russell, E., Gorokhovich, Y., & Kirsch, T. (2013). Disaster preparedness and humanitarian response in flood and landslide-affected communities in Eastern Uganda. *Disaster Prevention and management*.

Edwards, B., Allmann, B., Fäh, D., & Clinton, J. (2010). Automatic computation of moment magnitudes for small earthquakes and the scaling of local to moment magnitude. *Geophysical Journal International*, *183*(1), 407-420.

Engdahl, E., & Villaseñor, A. (2002). International handbook of earthquake and engineering seismology, Part A. In: London, UK: Academic Press.

Gardner, J., & Knopoff, L. (1974). Is the sequence of earthquakes in Southern California, with aftershocks removed, Poissonian? *Bulletin of the seismological society of America*, *64*(5), 1363-1367.

Graves, R., Jordan, T. H., Callaghan, S., Deelman, E., Field, E., Juve, G., Kesselman, C., Maechling, P., Mehta, G., & Milner, K. (2011). CyberShake: A physics-based seismic hazard model for southern California. *Pure and Applied Geophysics*, *168*(3), 367-381.

ISC. (2022). Seismological Centre, On-line Bulletin. *Int Seismol Cent, Thatcham, United Kingdom*. http://www.isc.ac.uk

Jacobs, L., Dewitte, O., Poesen, J., Delvaux, D., Thiery, W., & Kervyn, M. (2016). The Rwenzori Mountains, a landslide-prone region? *Landslides*, *13*(3), 519-536.

Kahuma, A., Kiggundu, B., Mwakali, J., & Taban-Wani, G. (2006). Building Material Aspects in Earthquake Resistant Construction in Western Uganda. Proceedings from the International Conference on Advances in Engineering and Technology,

Kato, S., & Mutonyi, R. (2011). The challenges of managing increasing landslides vulnerability on mount Elgon ecosystem. *Uganda: a case of human interactions with its environment on the verge of collapsing*.

Knapen, A., Kitutu, M. G., Poesen, J., Breugelmans, W., Deckers, J., & Muwanga, A. (2006). Landslides in a densely populated county at the footslopes of Mount Elgon (Uganda): characteristics and causal factors. *Geomorphology*, *73*(1-2), 149-165.

Kritikos, T., Robinson, T. R., & Davies, T. R. (2015). Regional coseismic landslide hazard assessment without historical landslide inventories: A new approach. *Journal of Geophysical Research: Earth Surface*, *120*(4), 711-729.

Loupekine, I. (1966). The Toro earthquake of 20 March 1966 and preliminary interpretation of seismograms: Uganda-(mission) 5-19 April 1966.

Maasha, N. (1975). The seismicity and tectonics of Uganda. *Tectonophysics*, *27*(4), 381-393.

Masaba, S., Mungai, D. N., Isabirye, M., & Nsubuga, H. (2017). Implementation of landslide disaster risk reduction policy in Uganda. *International journal of disaster risk reduction*, *24*, 326-331.

Midzi, V., Hlatywayo, D. J., Chapola, L. S., Kebede, F., Atakan, K., Lombe, D. K., Turyomurugyendo, G., & Tugume, F. A. (1999). Seismic hazard assessment in Eastern and Southern Africa. *Annals of Geophysics*, *42*(6).

Midzi, V., & Manzunzu, B. (2014). Large recorded earthquakes in sub-Saharan Africa. *Extreme natural hazards, disaster risks and societal implications*, *1*, 214.

Musson, R. M. (1999). Probabilistic seismic hazard maps for the North Balkan region. *Annals of Geophysics*, *42*(6).
Nakileza, B. R., & Nedala, S. (2020). Topographic influence on landslides characteristics and implication for risk management in upper Manafwa catchment, Mt Elgon Uganda. *Geoenvironmental Disasters*, *7*(1), 1-13.
NASA. (2022). *Rainfall-triggered landslides* https://gpm.nasa.gov/applications/landslides (Accessed 20/07/2022)
Pagani, M., Monelli, D., Weatherill, G., Danciu, L., Crowley, H., Silva, V., Henshaw, P., Butler, L., Nastasi, M., & Panzeri, L. (2014). OpenQuake engine: An open hazard (and risk) software for the global earthquake model. *Seismological Research Letters*, *85*(3), 692-702.
Petley, D. (2012). Global patterns of loss of life from landslides. *Geology*, *40*(10), 927-930.
Pezeshk, S., Zandieh, A., & Tavakoli, B. (2011). Hybrid empirical ground-motion prediction equations for eastern North America using NGA models and updated seismological parameters. *Bulletin of the seismological society of America*, *101*(4), 1859-1870.
Poggi, V., Durrheim, R., Tuluka, G. M., Weatherill, G., Gee, R., Pagani, M., Nyblade, A., & Delvaux, D. (2017). Assessing seismic hazard of the East African Rift: a pilot study from GEM and AfricaArray. *Bulletin of earthquake engineering*, *15*(11), 4499-4529.
Raines, G. L., Sawatzky, D. L., & Bonham-Carter, G. F. (2010). Expert Knowledge: New fuzzy logic tools in ArcGIS 10. www.esri.com
RCMRD. (2022). *Uganda 30 meters SRTM Digital Elevation ModelUganda 30 meters SRTM Digital Elevation Model* https://opendata.rcmrd.org/datasets/rcmrd::uganda-srtm-dem-30-meters/about (Accessed 15/07/2022)
Schlüter, T. (2008). *Geological atlas of Africa* (Vol. 307). Springer.
Stepp, J. (1972). Analysis of completeness of the earthquake sample in the Puget Sound area and its effect on statistical estimates of earthquake hazard. Proc. of the 1st Int. Conf. on Microzonazion, Seattle,
Storchak, D. A., Di Giacomo, D., Bondár, I., Engdahl, E. R., Harris, J., Lee, W. H., Villaseñor, A., & Bormann, P. (2013). Public release of the ISC–GEM global instrumental earthquake catalogue (1900–2009). *Seismological Research Letters*, *84*(5), 810-815.
Storchak, D. A., Di Giacomo, D., Engdahl, E., Harris, J., Bondár, I., Lee, W. H., Bormann, P., & Villaseñor, A. (2015). The ISC-GEM global instrumental earthquake catalogue (1900–2009): introduction. *Physics of the Earth and Planetary Interiors*, *239*, 48-63.
Styron, R., & Pagani, M. (2020). The GEM global active faults database. *Earthquake spectra*, *36*(1_suppl), 160-180.
Sykes, L. R. (1967). Mechanism of earthquakes and nature of faulting on the mid‐oceanic ridges. *Journal of Geophysical Research*, *72*(8), 2131-2153.
UBoS. (2020). Statistical Abstract. *Ministry of Finance, Planning and Economic Development, The Government of Uganda*, 14.
Uhrhammer, R. (1986). Characteristics of northern and central California seismicity. *Earthquake Notes*, *57*(1), 21.
USGS. (2022). *Repository of Earthquake-triggered Ground-failure Inventories* https://usgs.maps.arcgis.com/apps/webappviewer/index.html?id=2b6f1e57135f41028ea42ebc6813d967 (Accessed 23/07/2022)
van Stiphout, T., Zhuang, J., & Marsan, D. (2012). Seismicity declustering. *Community Online Resource for Statistical Seismicity Analysis*, *10*(1), 1-25.
Vicente, R., Parodi, S., Lagomarsino, S., Varum, H., & Silva, J. (2011). Seismic vulnerability and risk assessment: case study of the historic city centre of Coimbra, Portugal. *Bulletin of earthquake engineering*, *9*(4), 1067-1096.
Vilanova, S. P., Nemser, E. S., Besana‐Ostman, G. M., Bezzeghoud, M., Borges, J. F., Brum da Silveira, A., Cabral, J., Carvalho, J., Cunha, P. P., & Dias, R. P. (2014). Incorporating descriptive metadata into seismic source zone models for seismic‐hazard assessment: A case study of the Azores–West Iberian region. *Bulletin of the seismological society of America*, *104*(3), 1212-1229.
Weatherill, G., Pagani, M., & Garcia, J. (2014). OpenQuake ground motion toolkit—user guide, Global Earthquake Model (GEM). *Technical Report*.
Weatherill, G., Pagani, M., & Garcia, J. (2016). Exploring earthquake databases for the creation of magnitude-homogeneous catalogues: tools for application on a regional and global scale. *Geophysical Journal International*, *206*(3), 1652-1676.
Weichert, D. H. (1980). Estimation of the earthquake recurrence parameters for unequal observation periods for different magnitudes. *Bulletin of the seismological society of America*, *70*(4), 1337-1346.
Wiemer, S. (2001). A software package to analyze seismicity: ZMAP. *Seismological Research Letters*, *72*(3), 373-382.
Wiemer, S., & Wyss, M. (2000). Minimum magnitude of completeness in earthquake catalogs: Examples from Alaska, the western United States, and Japan. *Bulletin of the seismological society of America*, *90*(4), 859-869.
WorldBank, & GFDRR. (2022). *Global Landslide Hazard Map. Data Catalog* https://datacatalog.worldbank.org/search/dataset/0037584 (Accessed 27/07/2022)
Yilmaz, I. (2009). Landslide susceptibility mapping using frequency ratio, logistic regression, artificial neural networks and their comparison: a case study from Kat landslides (Tokat—Turkey). *Computers & Geosciences*, *35*(6), 1125-1138.